Letter

Discovery of 2,6-Dimethylpiperazines as Allosteric Inhibitors of CPS1

Alan Rolfe,* Shihua Yao, Toung-Vi Nguyen, Kiyoyuki Omoto, Federico Colombo, Milena Virrankoski, Frédéric H. Vaillancourt, Lihua Yu, Andrew Cook, Dominic Reynolds, Stephanos Ioannidis, Ping Zhu, Nicholas A. Larsen, and David M. Bolduc

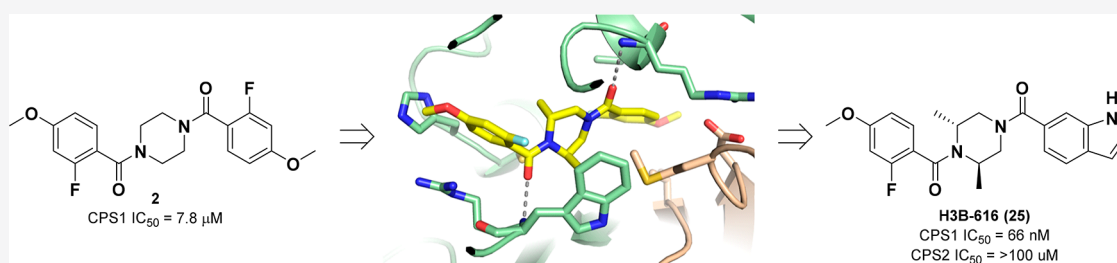Cite This: *ACS Med. Chem. Lett.* 2020, 11, 1305−1309

Read Online

ACCESS | Metrics & More | Article Recommendations | SI Supporting Information

ABSTRACT: Carbamoyl phosphate synthetase 1 (CPS1) is a potential synthetic lethal target in LKB1-deficient nonsmall cell lung cancer, where its overexpression supports the production of pyrimidine synthesis. In other cancer types, CPS1 overexpression and activity may prevent the accumulation of toxic levels of intratumoral ammonia to support tumor growth. Herein we report the discovery of a novel series of potent and selective small-molecule inhibitors of CPS1. Piperazine **2** was initially identified as a promising CPS1 inhibitor through a high-throughput screening effort. Subsequent structure−activity relationship optimization and structure-based drug design led to the discovery of piperazine H3B-616 (**25**), a potent allosteric inhibitor of CPS1 (IC$_{50}$ = 66 nM).

KEYWORDS: *Carbamoyl-phosphate synthetase 1, CPS1, allosteric inhibitors, high-throughput screening, cancer*

Carbamoyl phosphate synthetase 1 (CPS1) catalyzes the first step in ammonia detoxification through the urea cycle, generating carbamoyl phosphate from ammonia, bicarbonate, and two molecules of ATP.[1,2] In cancer, CPS1 can be overexpressed in several tumor lineages, where its activity is responsible for preventing the accumulation of toxic intratumoral ammonia in some cancer types,[3] while in others carbamoyl phosphate generated by CPS1 feeds into the pyrimidine biosynthetic pathway to support rapid tumor growth by maintaining a constant supply of pyrimidine nucleotides.[4−6] Overexpression of CPS1 is associated with poor prognosis in nonsmall cell lung cancer (NSCLC),[4,7] colon cancer,[8−10] cholangiocarcinoma,[11] and a subset of glioblastoma cancers,[12] indicating that multiple cancer types may exploit CSP1 overexpression to support aggressive tumor growth through these mechanisms. These observations suggest that small-molecule inhibitors of CPS1 may provide a therapeutic benefit for cancer patients in these indications.

We recently reported the identification of the first small-molecule inhibitor of CPS1, H3B-120 (**1**), through a high-throughput screening (HTS) campaign (Figure 1).[13] Kinetic studies and a cocrystal structure of inhibitor **1** bound to CPS1 demonstrated that **1** achieves selective CPS1 inhibition by binding to an allosteric pocket in the integrating domain. Binding to the allosteric pocket leads to a conformational
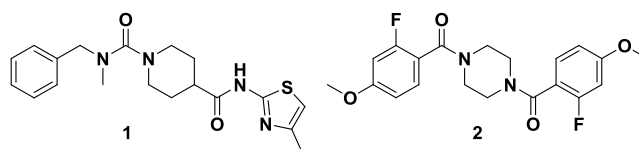

Figure 1. Structure of CPS1 inhibitors identified via HTS.

change in the carbamate synthetase domain, blocking ATP binding and subsequent catalysis. Furthermore, HTS hit compound **1** demonstrated CPS1 cellular target engagement by blocking CPS1 activity in both the urea cycle and support of the pyrimidine biosynthetic pathway.[13] However, the use of compound **1** as a biological tool to probe CPS1 cancer biology was limited by both its low potency (1.5 μM) and less desirable CYP-mediated metabolic stability and physicochemical properties.
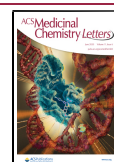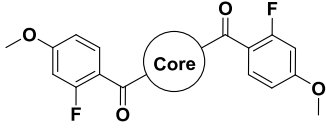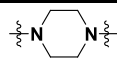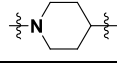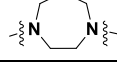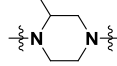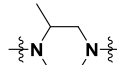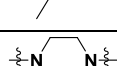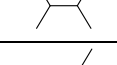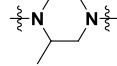
Herein we discuss the structure−activity relationship (SAR) of HTS hit **2**, a symmetrical piperazine with moderate activity (IC$_{50}$ = 7.8 μM) (Figure 1).[14] Initial SAR investigation focused on the exploration of the piperazine core, evaluating ring size, substituents, and stereochemistry (**3**−**12**, Table 1). Analogues

Table 1. Piperazine Core SAR Exploration

Cpd	Core	ADPGlo IC$_{50}$ (μM)[a]
2		7.8
3		21.5
4		18.9
5		5.2
6		6.3
7		36
8		11.4
9		>66
10		6.9
11		6.5
12		0.36

[a]IC$_{50}$ values were determined in a biochemical assay measuring ADP formation from CPS1 in the presence of the inhibitor. See the Supporting Information for methods. The reported IC$_{50}$ values are averages of at least two experimental replicates (N = 2).

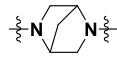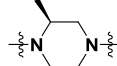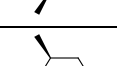were synthesized initially in a one-pot approach via bisacylation of various piperazine cores.[15−17] Alternatively, a stepwise approach using differentially protected piperazine cores could be employed for the rapid synthesis of unsymmetrical analogues.

Focusing on the piperazine core of **2**, removal of a single nitrogen atom (**3**) or expansion to the corresponding seven-membered diazepine ring (**4**) led to modest loss of activity,

while modification of the piperazine core through the addition of a methyl group (**5**) retained the activity. Further derivatization of the piperazine core with methyl substitution was tolerated for both the 2,6-dimethyl (**6**) and 2,5-dimethyl (**8**) analogues, while 2,3-disubstitution (**7**) or bridging of the piperazine (**9**) led to significant loss of inhibition. Building on the identification of **6**, we next investigated the effect of stereochemistry on the piperazine core by synthesizing all of the stereoisomers of **6**. While isomers **10** and **11** demonstrated activity comparable to that of the mixture **6**, the (2R,6R) isomer H3B-374 (**12**) exhibited an 18-fold enhancement in activity (IC$_{50}$ = 360 nM, H = 1.2).

Building on the discovery of **12**, we investigated the R$_1$ and R$_2$ amide SAR (**13**−**23**, Table 2). With regard to R$_1$ (**13**−**18**), increasing the size of the methoxy group to ethoxy led to a 2-fold improvement in activity (**13**), while replacement of the 4-methoxy with 4-methyl (**14**) or 4-F (**15**) led to significant loss of activity. Furthermore, switching the methoxy group from the 4-position to either the 3-position (**16**) or the 5-position (**17**) led to significant loss of activity. Alternatively, migration of the fluorine group from the 2-position to the 3-position (**18**) led to only a 2-fold loss of activity. With regard to R$_2$ (**19**−**23**), expansion of the 4-methoxy group to ethoxy (**19**) was tolerated, while a further increase in size to isopropoxy (**20**) led to significant loss of inhibition relative to **12**. Unlike R$_1$, replacement of 4-methoxy with 4-methyl (**21**) was tolerated, but loss of activity was observed upon substitution with 4-fluoro (**22**) or 5-methoxy (**23**). While the SAR generated gave us a better understanding of key structural features required for activity, further increases in potency by modification of R$_1$ and R$_2$ proved unfruitful.

To help understand the aforementioned SAR and enable further optimization, we solved a cocrystal structure of **12** bound to CPS1 at 2.62 Å resolution (Figure 2). The crystal structure reveals that **12** binds to an allosteric pocket in the integrating domain of CPS1, immediately adjacent to the ATP binding pocket of the carbamate synthesis domain. Comparison of the structure of **12** with the previously reported structure of **1** (PDB code 6UEL) shows that the two ligands bind in the same allosteric pocket.[13] Most of the interactions are hydrophobic, but there are also two key H-bonds formed between backbone amides of the protein (W776 and I851) and the pseudosymmetric amide oxygens on either side of the piperazine (Figure 2). These H-bonds dictate the ligand orientation in the pocket. Moreover, binding of inhibitor **12** to CPS1 stabilizes the flexible K loop (V653−H659) in a conformation that is not compatible with ATP binding and catalysis.[13] The conformation of this loop is stabilized by the salt bridge from D654 to R850 and by hydrophobic interactions from M656 to the ligand. This nonproductive conformation explains the inhibitory activity of the compound.

The piperazine core of **12** adopts a staggered flat confirmation that is enforced by the methyl groups at the 2- and 6-position, allowing R$_1$ and R$_2$ to make optimal interactions within the pocket. Hence, it can be rationalized that the lower IC$_{50}$ values for **7**, **8**, and **9** are due to the fact that the core is less amenable to the twisted conformation. Another interesting feature of the protein−ligand interaction is a CH−π engagement between the 2-Me of the piperazine and W776. With regard to R$_1$, the 4-OMe of **12** sits in a pocket created by V664, F890, I773, and I873, a hydrophobic interaction that leads to a 2-fold improvement in potency when R$_1$ is 4-OEt (**13**). However, the observed decrease in activity

Table 2. Initial Amide SAR for the (2R,6R)-2,6-Dimethylpiperazine Core

$R_2-N\diagdown\diagup N-R_1$

Cpd	R$_1$	R$_2$	ADPGlo IC$_{50}$ (μM)^a
12	*(structure)*	*(structure)*	0.36
13	*(structure)*	*(structure)*	0.13
14	*(structure)*	*(structure)*	2.2
15	*(structure)*	*(structure)*	2.6
16	*(structure)*	*(structure)*	>66
17	*(structure)*	*(structure)*	>66
18	*(structure)*	*(structure)*	0.54
19	*(structure)*	*(structure)*	0.38
20	*(structure)*	*(structure)*	1.4
21	*(structure)*	*(structure)*	0.36
22	*(structure)*	*(structure)*	1.3
23	*(structure)*	*(structure)*	5.1

^{a}IC$_{50}$ values were determined in a biochemical assay measuring ADP formation from CPS1 in the presence of the inhibitor. See the Supporting Information for methods. The reported IC$_{50}$ values are averages of at least two experimental replicates (N = 2).
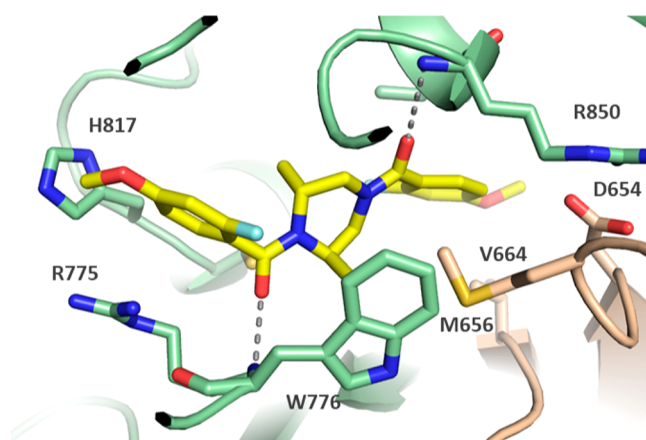

Figure 2. Crystal structure of H3B-374 (**12**) bound in the allosteric binding pocket of CPS1 (PDB code 6W2J). Green denotes residues from the integrating domain, and wheat color indicates those from the carbamate synthesis domain. The dashed lines indicate H-bonds to backbone amide nitrogens.
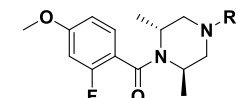
for **16** and **17** can be explained by the apparent clashes of the 3-OMe and 5-OMe groups with L813 and D654, respectively. The pocket of R$_2$ is partially solvent-exposed, which is consistent with the relatively tolerant SAR observed for **21** and **22**. However, the space around the 5-OMe substituent of **23** is restricted by H817, and this potential steric repulsion could explain the observed 14-fold loss of activity.
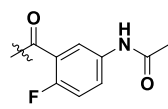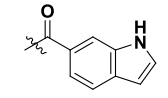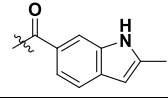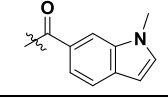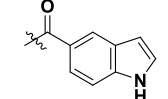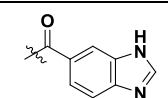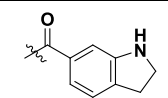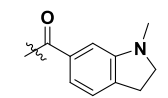
Having solved the cocrystal structure of **12** (Figure 2), we focused on optimizing its potency. D654 was identified from the cocrystal structure as a potential binding interaction that could be targeted through R$_1$ optimization. In this regard, analogues of **12** were designed to incorporate functional groups that could form a binding interaction with D654 (Table 3). While addition of the 5-acetamide (**24**) led to loss of activity, incorporation of 1H-indole (H3B-616, **25**; IC$_{50}$ = 66 nM, H = 1.4) at R$_1$ led to a 5-fold improvement in potency relative to **12**. Likewise, the corresponding 2-methyl-1H-indole analogue **26** exhibited an improvement in activity, though the bulkier substituent was slightly less tolerated. To help demonstrate this SAR, N-methylindole **27** was synthesized and, as predicted, was not tolerated (IC$_{50}$ = 31 μM). This was further demonstrated with the indole regioisomer **28** which negated the gain in activity through Asp654 binding. Furthermore, expansion of the SAR to the corresponding imidazole **29**, indoline **30**, and 1-methylindoline **31** analogues did not result in any significant gain in activity.

CPS1 is one of two genes with carbamoyl phosphate synthetase activity in the human genome, the second gene being CAD. CAD is a trifunctional enzyme that catalyzes the first three steps of de novo pyrimidine synthesis and exhibits CPS2, aspartate transcarbamoylase, and dihydroorotase activity. Since CAD facilitates de novo pyrimidine synthesis in most cell types, a nonselective CPS inhibitor would be expected to encounter toxicity issues associated with CPS2 inhibition. We therefore assessed the selectivity of compound H3B-616 (**25**) by measuring inhibition of the carbamoyl phosphate synthetase activity of CPS1 and CPS2 in a biochemical assay.[13] While **25** robustly inhibited CPS1 (IC$_{50}$ = 0.066 μM), it demonstrated no appreciable inhibition of CPS2 (IC$_{50}$ ≥ 100 μM).

We previously demonstrated targeted cellular inhibition of CPS1 by measuring inhibition of urea production from

Table 3. SAR Exploration Targeting Asp654

Cpd	R$_1$	ADPGlo IC$_{50}$ (µM)[a]
24		>66
25		0.066
26		0.17
27		31.0
28		>66
29		4.9
30		6.4
31		7.7

[a]IC$_{50}$ values were determined in a biochemical assay measuring ADP formation from CPS1 in the presence of the inhibitor. See the Supporting Information for methods. The reported IC$_{50}$ values are averages of at least two experimental replicates (N = 2).
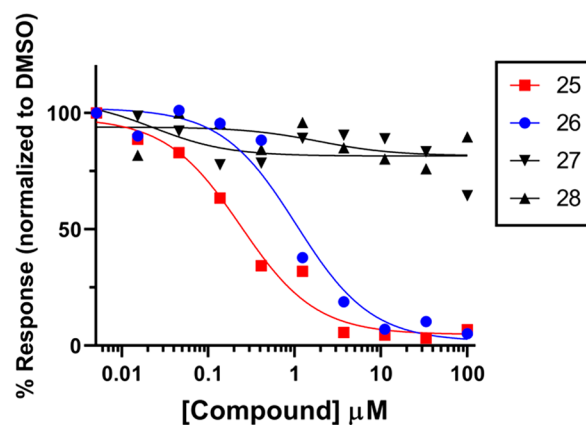

Figure 3. Targeted cellular inhibition of CPS1 activity. Inhibition of urea production from primary human hepatocytes by **25**, **26**, **27**, and **28** is shown. Primary human hepatocytes were incubated with 10 mM NH$_4$Cl in the presence of compound at the indicated concentration. Urea secreted into the medium was measured after 16 h. The data are provided as a representative graph. Replicate experiments yielded similar results.

the application of this tool compound in the context of liver kinase B1 (LKB1)-deficient NSCLC.

ASSOCIATED CONTENT

Supporting Information

The Supporting Information is available free of charge at https://pubs.acs.org/doi/10.1021/acsmedchemlett.0c00145.

Experimental details, spectral data for selected compounds, X-ray crystallographic analysis, and biological assay protocols (PDF)

Accession Codes

The coordinates have been deposited in the PDB with accession code 6W2J.

AUTHOR INFORMATION

Corresponding Author

Alan Rolfe — H3 Biomedicine Inc., Cambridge, Massachusetts 02139, United States; orcid.org/0000-0002-3265-1022; Phone: 1 617-252-5026; Email: alan_rolfe@h3biomedicine.com

Authors

Shihua Yao — H3 Biomedicine Inc., Cambridge, Massachusetts 02139, United States

Toung-Vi Nguyen — H3 Biomedicine Inc., Cambridge, Massachusetts 02139, United States

Kiyoyuki Omoto — H3 Biomedicine Inc., Cambridge, Massachusetts 02139, United States

Federico Colombo — H3 Biomedicine Inc., Cambridge, Massachusetts 02139, United States

Milena Virrankoski — H3 Biomedicine Inc., Cambridge, Massachusetts 02139, United States

Frédéric H. Vaillancourt — H3 Biomedicine Inc., Cambridge, Massachusetts 02139, United States

Lihua Yu — H3 Biomedicine Inc., Cambridge, Massachusetts 02139, United States

Andrew Cook — H3 Biomedicine Inc., Cambridge, Massachusetts 02139, United States

Dominic Reynolds — H3 Biomedicine Inc., Cambridge, Massachusetts 02139, United States

primary human hepatocytes treated with CPS1 inhibitors.[13] In this cellular assay, biochemically active compounds **25** and **26** demonstrated robust cellular inhibition of CPS1 with IC$_{50}$ values of 0.24 µM and 1.0 µM, respectively, while biochemically inactive compounds **27** and **28** showed no activity (Figure 3).

In summary, we have identified and developed a series of allosteric small-molecule inhibitors of carbamoyl phosphate synthetase 1 (CPS1). Starting from HTS hit **2** (IC$_{50}$ = 7.8 µM), initial SAR followed by structure-based drug design furnished CPS1 inhibitor H3B-616 (**25**) with potent biochemical (IC$_{50}$ = 66 nM) and cellular (IC$_{50}$ = 240 nM) activity. A cocrystal structure of **12** bound to CPS1 demonstrated an allosteric pocket in the integrating domain. In comparison to our previously reported inhibitor **1**, **25** demonstrated improved biochemical potency (66 nM vs 1.5 µM) and a significant improvement in human hepatocyte stability (8.7 vs 35 µL/min/10-6 cells), favorable permeability (Caco2 A-B = 12.3 × 10^{-6} cm/s), and good kinetic solubility (148 µM, pH 7.4). Further studies are ongoing to investigate

Stephanos Ioannidis − H3 Biomedicine Inc., Cambridge, Massachusetts 02139, United States

Ping Zhu − H3 Biomedicine Inc., Cambridge, Massachusetts 02139, United States

Nicholas A. Larsen − H3 Biomedicine Inc., Cambridge, Massachusetts 02139, United States

David M. Bolduc − H3 Biomedicine Inc., Cambridge, Massachusetts 02139, United States; orcid.org/0000-0003-2003-8631

Complete contact information is available at:
https://pubs.acs.org/10.1021/acsmedchemlett.0c00145

Author Contributions

The manuscript was written through contributions of all authors.

◼ ABBREVIATIONS

CPS1, carbamoyl-phosphate synthase 1; HTS, high-throughput screening; Bn, benzyl; SAR, structure−activity relationship

◼ REFERENCES

(1) Adeva, M. M.; Souto, G.; Blanco, N.; Donapetry, C. Ammonium Metabolism in Humans. *Metab., Clin. Exp.* **2012**, *61*, 1495−1511.

(2) de Cima, S.; Polo, L. M.; Díez-Fernández, C.; Martínez, A. I.; Cervera, J.; Fita, I.; Rubio, V. Structure of Human Carbamoyl Phosphate Synthetase: Deciphering the on/off Switch of Human Ureagenesis. *Sci. Rep.* **2015**, *5*, 16950.

(3) Li, L.; Mao, Y.; Zhao, L.; Li, L.; Wu, J.; Zhao, M.; Du, W.; Yu, L.; Jiang, P. P53 Regulation of Ammonia Metabolism through Urea Cycle Controls Polyamine Biosynthesis. *Nature* **2019**, *567* (7747), 253−256.

(4) Kim, J.; Hu, Z.; Cai, L.; Li, K.; Choi, E.; Faubert, B.; Bezwada, D.; Rodriguez-Canales, J.; Villalobos, P.; Lin, Y.-F.; et al. CPS1 Maintains Pyrimidine Pools and DNA Synthesis in KRAS/LKB1-Mutant Lung Cancer Cells. *Nature* **2017**, *546*, 168−172.

(5) Çeliktaş, M.; Tanaka, I.; Chandra Tripathi, S.; Fahrmann, J. F.; Aguilar-Bonavides, C.; Villalobos, P.; Delgado, O.; Dhillon, D.; Dennison, J. B.; Ostrin, E. J.; et al. Role of CPS1 in Cell Growth, Metabolism, and Prognosis in LKB1-Inactivated Lung Adenocarcinoma. *J. Natl. Cancer Inst.* **2017**, *109*, djw231.

(6) Lee, J. S.; Adler, L.; Karathia, H.; Carmel, N.; Rabinovich, S.; Auslander, N.; Keshet, R.; Stettner, N.; Silberman, A.; Agemy, L.; et al. Urea Cycle Dysregulation Generates Clinically Relevant Genomic and Biochemical Signatures. *Cell* **2018**, *174*, 1559−1570.

(7) Pham-Danis, C.; Gehrke, S.; Danis, E.; Rozhok, A. I.; Daniels, M. W.; Gao, D.; Collins, C.; Paola, J. T. D.; D'Alessandro, A.; DeGregori, J. Urea Cycle Sustains Cellular Energetics upon EGFR Inhibition in EGFR-Mutant NSCLC. *Mol. Cancer Res.* **2019**, *17*, 1351−1364.

(8) May, D.; Pan, S.; Crispin, D. A.; Lai, K.; Bronner, M. P.; Hogan, J.; Hockenbery, D. M.; McIntosh, M.; Brentnall, T. A.; Chen, R. Investigating Neoplastic Progression of Ulcerative Colitis with Label-Free Comparative Proteomics. *J. Proteome Res.* **2011**, *10*, 200−209.

(9) Palaniappan, A.; Ramar, K.; Ramalingam, S. Computational Identification of Novel Stage-Specific Biomarkers in Colorectal Cancer Progression. *PLoS One* **2016**, *11*, No. e0156665.

(10) Lee, Y.-Y.; Li, C.-F.; Lin, C.-Y.; Lee, S.-W.; Sheu, M.-J.; Lin, L.-C.; Chen, T.-J.; Wu, T.-F.; Hsing, C.-H. Overexpression of CPS1 Is an Independent Negative Prognosticator in Rectal Cancers Receiving Concurrent Chemoradiotherapy. *Tumor Biol.* **2014**, *35*, 11097−11105.

(11) Ma, S.-L.; Li, A.-J.; Hu, Z.-Y.; Shang, F.-S.; Wu, M.-C. Co-Expression of the Carbamoyl-Phosphate Synthase 1 Gene and Its Long Non-Coding RNA Correlates with Poor Prognosis of Patients with Intrahepatic Cholangiocarcinoma. *Mol. Med. Rep.* **2015**, *12*, 7915−7926.

(12) Milinkovic, V.; Bankovic, J.; Rakic, M.; Stankovic, T.; Skender-Gazibara, M.; Ruzdijic, S.; Tanic, N. Identification of Novel Genetic Alterations in Samples of Malignant Glioma Patients. *PLoS One* **2013**, *8*, e82108.

(13) Yao, S.; Nguyen, T.-V.; Rolfe, A.; Agrawal, A. A.; Ke, J.; Peng, S.; Colombo, F.; Yu, S.; Bouchard, P.; Wu, J.; Huang, K.-C.; Bao, X.; Omoto, K.; Selvaraj, A.; Yu, L.; Ioannidis, S.; Vaillancourt, F. H.; Zhu, P.; Larsen, N. A.; Bolduc, D. M. Small molecule inhibition of CPS1 activity through an allosteric pocket. *Cell Chem. Biol.* **2020**, *27*, 259−268.

(14) **2** was identified from a biochemical high-throughput screen of ∼350 000 compounds after a series of counterscreens and biophysical assays to verify direct binding.

(15) Wang, Y.; Zhang, Z.; Meanwell, A. N. Regioselective Monobenzoylation of Unsymmetrical Piperazines. *J. Org. Chem.* **2000**, *65*, 4740−4742.

(16) Wang, T.; Kadow, J. F.; Zhang, Z.; Yin, Z.; Gao, Q.; Wu, D.; Parker, D. D.; Yang, Z.; Zadjura, L.; Robinson, B. A.; Gong, Y.-F.; Blair, W. S.; Shi, P.-Y.; Yamanaka, G.; Lin, P.-F.; Meanwell, N. A. Inhibitors of HIV-1 attachment. Part 4: A study of the effect of piperazine substitution patterns on antiviral potency in the context of indole-based derivatives. *Bioorg. Med. Chem. Lett.* **2009**, *19*, 5140−5145.

(17) Liu, F.; Dawadi, S.; Maize, K. M.; Dai, R.; Park, S. W.; Schnappinger, D.; Finzel, B. C.; Aldrich, C. C. Structure-Based Optimization of Pyridoxal 5′-Phosphate-Dependent Transaminase Enzyme (BioA) Inhibitors that Target Biotin Biosynthesis in Mycobacterium tuberculosis. *J. Med. Chem.* **2017**, *60*, 5507−5520.